

## Biaxial stress-dependent optical band gap, crystalline, and electronic structure in wurtzite ZnO: Experimental and ab initio study

Y. F. Li, B. Yao, Y. M. Lu, Y. Q. Gai, C. X. Cong et al.

Citation: *J. Appl. Phys.* **104**, 083516 (2008); doi: 10.1063/1.3000601

View online: <http://dx.doi.org/10.1063/1.3000601>

View Table of Contents: <http://jap.aip.org/resource/1/JAPIAU/v104/i8>

Published by the [American Institute of Physics](#).

---

### Related Articles

Tribological properties of nanocrystalline diamond films deposited by hot filament chemical vapor deposition  
[AIP Advances 2, 032164 \(2012\)](#)

The combined effect of surface roughness and internal stresses on nanoindentation tests of polysilicon thin films  
[J. Appl. Phys. 112, 044512 \(2012\)](#)

Mechanism for atmosphere dependence of laser damage morphology in HfO<sub>2</sub>/SiO<sub>2</sub> high reflective films  
[J. Appl. Phys. 112, 023111 \(2012\)](#)

Superhard behaviour, low residual stress, and unique structure in diamond-like carbon films by simple bilayer approach  
[J. Appl. Phys. 112, 023518 \(2012\)](#)

Ultrafast photoinduced mechanical strain in epitaxial BiFeO<sub>3</sub> thin films  
[Appl. Phys. Lett. 101, 041902 \(2012\)](#)

---

### Additional information on J. Appl. Phys.

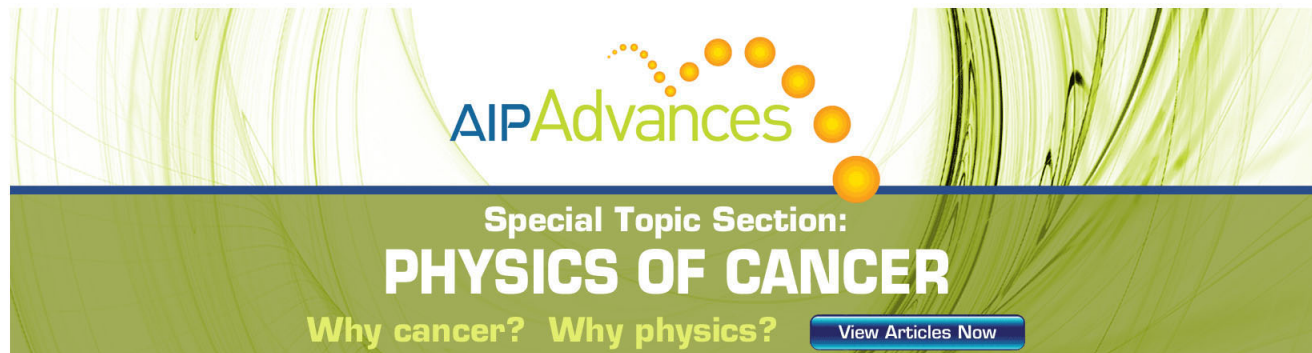
Journal Homepage: <http://jap.aip.org/>

Journal Information: [http://jap.aip.org/about/about\\_the\\_journal](http://jap.aip.org/about/about_the_journal)

Top downloads: [http://jap.aip.org/features/most\\_downloaded](http://jap.aip.org/features/most_downloaded)

Information for Authors: <http://jap.aip.org/authors>

## ADVERTISEMENT



**AIPAdvances**

Special Topic Section:  
**PHYSICS OF CANCER**

Why cancer? Why physics? [View Articles Now](#)

# Biaxial stress-dependent optical band gap, crystalline, and electronic structure in wurtzite ZnO: Experimental and *ab initio* study

Y. F. Li,<sup>1,2,a)</sup> B. Yao,<sup>1,b)</sup> Y. M. Lu,<sup>1</sup> Y. Q. Gai,<sup>1,2</sup> C. X. Cong,<sup>1</sup> Z. Z. Zhang,<sup>1</sup> D. X. Zhao,<sup>1</sup> J. Y. Zhang,<sup>1</sup> B. H. Li,<sup>1</sup> D. Z. Shen,<sup>1</sup> X. W. Fan,<sup>1</sup> and Z. K. Tang<sup>3</sup>

<sup>1</sup>Laboratory of Excited State Processes, Changchun Institute of Optics, Fine Mechanics and Physics, Chinese Academy of Sciences, Changchun 130033, People's Republic of China

<sup>2</sup>Graduate School of Chinese Academy of Sciences, Beijing 100039, People's Republic of China

<sup>3</sup>Department of Physics, Hong Kong University of Science and Technology, Clear Water Bay, Kowloon, Hong Kong

(Received 24 February 2008; accepted 31 August 2008; published online 27 October 2008)

The relationship between band gap and biaxial stress in wurtzite ZnO thin films has been investigated by side-inclination x-ray diffraction technique and optical absorbance spectrum as well as *ab initio* calculation. The experimental result shows that differing from other semiconductor thin films with hexagonal structure, such as GaN, the band gap of ZnO thin films increases with the increase in biaxial tensile stress. For explaining the difference, *ab initio* calculation is performed to simulate the relationship between band gap and biaxial stress of wurtzite ZnO and GaN. The calculated result indicates that the band gap of ZnO increases under biaxial tensile stress but GaN is opposite, supporting our experimental result. The band offset calculation shows that the conduction-band minimum (CBM) and the valence-band maximum (VBM) of ZnO and GaN offset to low energy under biaxial tensile stress. The VBM offset of ZnO is larger than the CBM, responsible for the increase in band gap. The VBM offset of GaN is smaller than the CBM, responsible for the decrease in band gap. The difference between ZnO and GaN is attributed to the strong *p-d* coupling in valence band of ZnO, but strong *p-p* coupling in valence band of GaN.

© 2008 American Institute of Physics. [DOI: 10.1063/1.3000601]

## I. INTRODUCTION

Zinc oxide (ZnO), as a direct wide band gap semiconductor material, has attracted much attention for many years because of their excellent performance in blue-ultraviolet (UV) and UV region.<sup>1</sup> The research for ZnO-based light emitting devices (LEDs) and laser diodes (LDs) has been made great progress recent years.<sup>2–9</sup> The performance of these LEDs and LDs are strongly dependent on quality of thin films. However, ZnO films are usually heteroepitaxially grown on insulated substrate or semiconductor. It is inevitable that stress (or strain) appears in the film in heteroepitaxial growth process due to lattice mismatch and the thermal expansion coefficient difference between the substrate and the film. Under some conditions, biaxial stress badly influence on crystalline quality of thin film and performance of LEDs. Furthermore, biaxial stress also affects physical properties of thin film, such as optical and electrical properties. Therefore, for well understanding effect of biaxial stress on these properties of ZnO films, it is necessary to measure biaxial stress in ZnO films and study its effect on some physical properties.

Another UV optoelectronic material, gallium nitride (GaN), is similar with ZnO in some aspects, for example, crystalline structure, band gap of about 3.4 eV at room temperature, preferential orientation in the *c*-axis direction on some substrates, and so on. Also, because GaN has been

researched for a long time and GaN-based LEDs and LDs had realized commercial product,<sup>10</sup> the research of ZnO can draw lessons from the experience of GaN research. Meanwhile, by comparing study of ZnO and GaN, the trend of some properties of III-V and II-VI groups can be understood. Similar to ZnO, biaxial stress also affects on some properties of GaN thin film. Hence, by comparing the similarities and differences of ZnO and GaN under biaxial stress, it benefits for further understanding their properties.

On the other hand, some researchers have reported some properties of ZnO and GaN under isotropy hydrostatic pressure recent years, such as electronic, elastic, lattice dynamic, and optical properties.<sup>11–16</sup> Under isotropy hydrostatic pressure, both *a*-axis and *c*-axis lattice constants decrease, namely, the strains in the *a*- and *c*-axis directions are compressive strains. Differing from hydrostatic pressure, biaxial stress is not a three-dimensional stress but a two-dimensional stress paralleled to the film surface because the films are free in the direction vertical to surface. For instance, ZnO and GaN thin films usually grown on some substrates such *c*-sapphire (0001), quartz, and GaAs (111) generally are under biaxial tensile stress because the lattice mismatch or thermal mismatch between film and substrate. The strain in *c*-axis direction is compressive when the thin films are under biaxial tensile stress because of the Poisson effect. Thus, the properties of thin films under biaxial stress are different with the ones under hydrostatic pressure. Moreover, there are few comparing studies on effect of biaxial stress on properties of ZnO and GaN thin films. Thus, it is also very necessary to

<sup>a)</sup>Electronic mail: yongfengli@yahoo.com.cn.

<sup>b)</sup>Author to whom correspondence should be addressed. Electronic mail: yaobin196226@yahoo.com.cn.

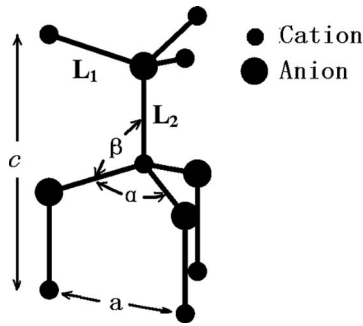


FIG. 1. A primitive cell plot of a wurtzite structure.

study some properties of ZnO and GaN thin films under biaxial stress because thin films are commonly subjected to biaxial stress.

In this paper, the biaxial stress of ZnO thin films is characterized by side-inclination x-ray diffraction (XRD) technique. The optical absorbance spectrum is performed to measure optical band gap of ZnO. The relationship between band gap and biaxial stress of ZnO is determined. The experimental result is well supported by *ab initio* calculation. On effect of biaxial stress on band gap, the difference between ZnO and GaN is also discussed in the frame of density functional theory (DFT).

## II. ELASTIC CONSTANTS AND THE CHARACTERIZATION METHOD OF BIAXIAL STRESS OF ZINC OXIDE THIN FILMS

### A. Elastic constants of wurtzite ZnO

ZnO has hexagonal structures with two lattice constants  $a$  and  $c$ , as shown in Fig. 1. The strains paralleled to  $a$ - and  $c$ -axes can be defined as the following, respectively:

$$\varepsilon_{11} = \varepsilon_{22} = \frac{a - a_0}{a}, \quad (1a)$$

$$\varepsilon_{33} = \frac{c - c_0}{c}. \quad (1b)$$

The elastic constants reflect the relation between stress and strain in Hook's law. For the crystal with wurtzite structure under normal stress, Hook's law can be expressed as the following matrix form:

$$(\sigma_{ij}) = (C_{ik})(\varepsilon_{kj}), \quad i, j, k = 1, 2, 3, \quad (2)$$

where  $\sigma_{ij}$  and  $\varepsilon_{ij}$  are the elements of stress and strain tensor. Their main diagonal elements ( $\sigma_{ii}$  and  $\varepsilon_{ii}$ ) are the normal stress and strain, respectively. The nondiagonal elements  $\sigma_{ij}$  and  $\varepsilon_{ij}$  ( $i \neq j$ ) can be zero by choosing appropriated coordinate frame. The matrix elements  $C_{ij}$  represent the elastic constants. Only five of the nine elements  $C_{ij}$  are independent due to the symmetry of wurtzite ZnO and they are  $C_{11}$ ,  $C_{12}$ ,  $C_{13}$ ,  $C_{33}$ , and  $C_{44}$ .

For a uniaxial stress paralleled to the  $c$ -axis ( $\sigma_{11} = \sigma_{22} = 0$ ), the Poisson ratio is defined as  $\nu = \varepsilon_{11} / \varepsilon_{33}$ . The relation between  $\nu$  and the stiffness constant  $C_{ij}$  can be expressed as

$$\nu = \frac{C_{13}}{C_{11} + C_{12}}. \quad (3)$$

For an isotropic biaxial stress ( $\sigma_{11} = \sigma_{22}$ ) perpendicular to the  $c$ -axis, the biaxial relaxation coefficient  $R^B$  is defined as  $R^B = \varepsilon_{33} / \varepsilon_{11}$ . Moreover the relation between  $R^B$  and the stiffness constant  $C_{ij}$  is given by

$$R^B = \frac{2C_{13}}{C_{33}}. \quad (4)$$

For an isotropic elastic body, Hooke law can be written as

$$\varepsilon_{11} = \frac{1}{E}\sigma_{11} - \frac{\nu}{E}\sigma_{22} - \frac{\nu}{E}\sigma_{33}, \quad (5a)$$

$$\varepsilon_{22} = -\frac{\nu}{E}\sigma_{11} + \frac{1}{E}\sigma_{22} - \frac{\nu}{E}\sigma_{33}, \quad (5b)$$

$$\varepsilon_{33} = -\frac{\nu}{E}\sigma_{11} - \frac{\nu}{E}\sigma_{22} + \frac{1}{E}\sigma_{33}, \quad (5c)$$

where  $\sigma_{11}$ ,  $\sigma_{22}$ , and  $\sigma_{33}$  are the diagonal elements of the stress tensor, and  $\varepsilon_{11}$ ,  $\varepsilon_{22}$ ,  $\varepsilon_{33}$  are the diagonal elements of the strain tensor.  $E$  and  $\nu$  are Young's modulus and Poisson ratio.

For an isotropic biaxial stress, it is reasonable to assume the stress paralleled to the normal direction of film surface is zero, namely,  $\sigma_{zz} = 0$ . The following equation can be obtained from Eq. (5):

$$\frac{\varepsilon_{33}}{\varepsilon_{11}} = -R^B = -\frac{2\nu}{1 - \nu}. \quad (6)$$

Combining Eqs. (3), (4), and (6), it is concluded that stiffness constants  $C_{11}$ ,  $C_{12}$ ,  $C_{13}$ , and  $C_{33}$  satisfy the following equation for an isotropic elastic body:

$$C_{11} + C_{12} - C_{13} - C_{33} = 0. \quad (7)$$

The elastic constants of ZnO,  $C_{11}$ ,  $C_{22}$ ,  $C_{12}$ , and  $C_{13}$  from our calculation, and reported in some literatures are listed in Table I. The calculation detail will be seen in Sec. IV. Our calculated result is closer to experimental and others' calculated ones. The expression  $C_{11} + C_{12} - C_{13} - C_{33}$ , Young's modulus  $E$ , Poisson ratio  $\nu$ , and biaxial relaxation coefficient  $R^B$  are also listed in Table I. The expression  $C_{11} + C_{12} - C_{13} - C_{33}$  is very small, even near zero. So, it is reasonable to assume that wurtzite ZnO is an isotropic elastic body and obeys Hooke law expressed by formula (5). This result is necessary for measuring biaxial stress of thin film by side-inclination XRD technique. In Sec. II B, the principle of side-inclination XRD technique will be introduced. Additionally, the elastic constants of wurtzite GaN is also calculated and listed in Table I for comparing with ZnO. It is found that for GaN, the expression  $C_{11} + C_{12} - C_{13} - C_{33}$  is also very small. This indicates that wurtzite GaN obeys Hooke law expressed by formula (5) and it is also suitable for GaN to measure its biaxial stress using the side-inclination XRD technique.

TABLE I. Calculated elastic constants (in GPa) of wurtzite ZnO and GaN compared with results of other first-principle calculations and measurements.

|                    | $C_{11}$ | $C_{12}$ | $C_{13}$ | $C_{33}$ | $C_{11}+C_{12}-C_{13}-C_{13}$ | $E$ | $R^B$ | $\nu$ |
|--------------------|----------|----------|----------|----------|-------------------------------|-----|-------|-------|
| ZnO                |          |          |          |          |                               |     |       |       |
| Present            | 198      | 113      | 96       | 210      | 5                             | 151 | 0.915 | 0.309 |
| Calc. <sup>a</sup> | 218      | 137      | 121      | 229      | 5                             | 147 | 1.057 | 0.341 |
| Calc. <sup>b</sup> | 226      | 139      | 123      | 242      | 0                             | 159 | 1.017 | 0.337 |
| Calc. <sup>c</sup> | 246      | 127      | 105      | 246      | 22                            | 187 | 0.854 | 0.282 |
| Expt. <sup>d</sup> | 210      | 121      | 105      | 211      | 15                            | 144 | 0.995 | 0.317 |
| Expt. <sup>e</sup> | 207      | 118      | 106      | 210      | 9                             | 141 | 1.001 | 0.326 |
| Expt. <sup>f</sup> | 190      | 110      | 90       | 196      | 14                            | 140 | 0.918 | 0.300 |
| GaN                |          |          |          |          |                               |     |       |       |
| Present            | 335      | 118      | 82       | 371      | -1                            | 341 | 0.442 | 0.181 |
| Calc. <sup>g</sup> | 367      | 135      | 103      | 405      | -6                            | 363 | 0.509 | 0.205 |
| Calc. <sup>h</sup> | 350      | 140      | 104      | 376      | 10                            | 332 | 0.553 | 0.212 |
| Calc. <sup>i</sup> | 431      | 109      | 64       | 476      | 0                             | 461 | 0.269 | 0.119 |
| Expt. <sup>j</sup> | 370      | 145      | 110      | 390      | 15                            | 343 | 0.564 | 0.214 |
| Expt. <sup>k</sup> | 365      | 135      | 114      | 381      | 5                             | 329 | 0.598 | 0.228 |

<sup>a</sup>Reference 17.

<sup>b</sup>Reference 18.

<sup>c</sup>Reference 19.

<sup>d</sup>Reference 20.

<sup>e</sup>Reference 21.

<sup>f</sup>Reference 22.

<sup>g</sup>Reference 23.

<sup>h</sup>Reference 24.

<sup>i</sup>Reference 25.

<sup>j</sup>Reference 26.

<sup>k</sup>Reference 27.

## B. Principle of side-inclination x-ray diffraction technique

The geometrical relationship between the Cartesian coordinates ( $x, y, z$ ) and sphere coordinates ( $r, \psi, \varphi$ ) is shown in Fig. 2 and expressed as follows:

$$x = r \sin \psi \cos \varphi, \quad (8a)$$

$$y = r \sin \psi \sin \varphi, \quad (8b)$$

$$z = r \cos \psi, \quad (8c)$$

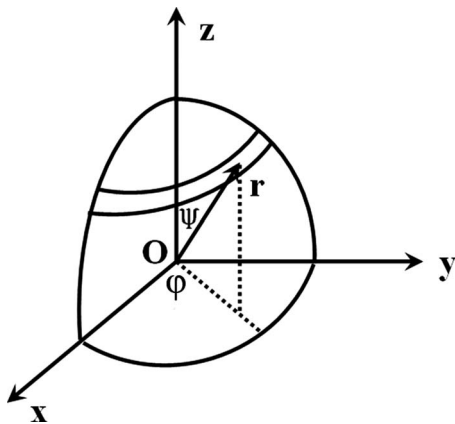


FIG. 2. Relationship between the Cartesian coordinates ( $x, y, z$ ) and sphere coordinates.

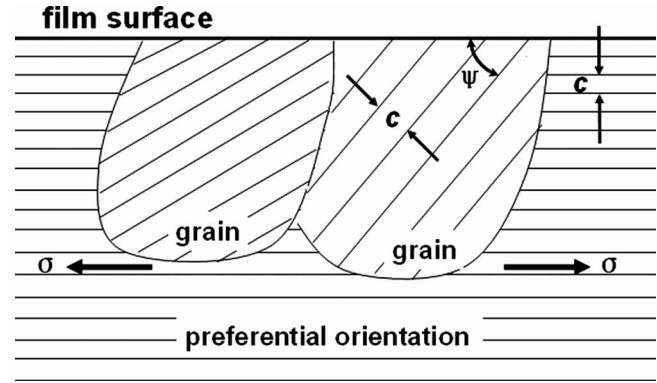


FIG. 3. Principle of side-inclination XRD method.

$$r^2 = x^2 + y^2 + z^2. \quad (8d)$$

Using differential equation of Eq. (8),  $\varepsilon_{11} = \varepsilon_{22} = (dx/x) = (dy/y)$ ,  $\varepsilon_{33} = (dz/z)$ , and  $\varepsilon_\psi = (dr/r)$ , we can obtain the equation

$$\varepsilon_\psi = \varepsilon_{11} \cos^2 \psi + \varepsilon_{33} \sin^2 \psi. \quad (9)$$

When the normal direction of diffraction planar parallels to the vector  $\mathbf{r}$ , namely, the angle between diffraction planar and sample surface is  $\psi$ . Considering differential Bragg's equation, the strain  $\varepsilon_\psi$  along the  $\mathbf{r}$  direction can be calculated by the following equation:

$$\varepsilon_\psi = \frac{d_\psi - d_0}{d_0} = \frac{\Delta d}{d_0} = -\frac{\pi}{180} \cot \theta_0 \Delta \theta, \quad (10)$$

where  $d_\psi$ ,  $d_0$ ,  $\theta_0$ , and  $\Delta \theta$  are the interplanar spacing perpendicular to the vector  $\mathbf{r}$ , interplanar spacing of stress-free sample, diffraction angle of stress-free sample, and diffraction angle shift corresponding to stress-free sample, respectively. Because the biaxial stress is axis-symmetry perpendicular to the sample surface (the planar O-xy in Fig. 2), there exists  $\sigma_{11} = \sigma_{22}$  and  $\sigma_{33} = 0$ . In combined Eqs. (5), (9), and (10), we can obtain the formula used to calculating biaxial stress,

$$\sigma_{11} = -\frac{E}{2(1+\nu)} \frac{\pi}{180} \cot \theta_0 \frac{\partial(2\theta)}{\partial \sin^2 \psi}. \quad (11)$$

Figure 3 shows the principle of side-inclination XRD method measuring biaxial stress of thin films. Although ZnO and GaN thin films are with  $c$ -axis preferential orientation, the  $c$ -axis offsets inevitably from the normal direction of thin film surface in a few grains (the offset angle  $\psi$ ). If the thin film is subjected to biaxial stress, the lattice constant  $c$  in these grains is different with one perpendicular to thin film surface. The difference increases with the increase in the offset angle. In the XRD experiment, the lattice constant  $c$  perpendicular to thin film surface can be obtained when  $\theta-2\theta$  scan is performed. The thin film is turned to the angle  $\psi$ , the lattice constant  $c$  with the offset angle  $\psi$  also be obtained by  $\theta-2\theta$  scan. In this way, the biaxial stress of thin film can be measured by Eq. (11).



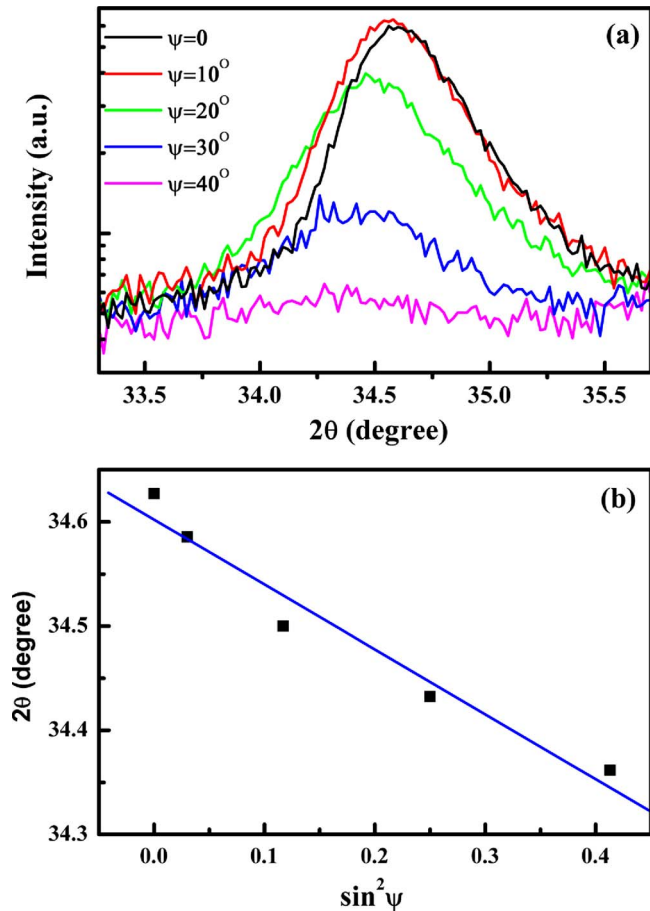


FIG. 4. (Color online) (a) XRD plot of ZnO under different inclination angle  $\psi$  and (b) (0002) diffraction peak position as a function of  $\sin^2 \psi$ .

### III. EXPERIMENTAL STUDY OF THE RELATIONSHIP BETWEEN BAND GAP AND BIAxIAL STRESS OF ZINC OXIDE THIN FILMS

#### A. Experimental detail

ZnO thin films were grown on quartz substrate 240 °C by radio frequency (rf) magnetic sputtering. The sample is cut into four pieces and three of them are annealed under O<sub>2</sub> atmosphere at 400, 600, and 800 °C for 30 min. Experimental detail can be seen in our previous work.<sup>28</sup> The choice of diffraction peak used to measure biaxial stress is important in side-inclination XRD technique because its position and intensity directly influence the measured precision. In our previous work, the (213) diffraction peak with large angle was used to measure the biaxial stress because diffraction peak with large angle benefits for enhancing precision owing to differential Bragg's equation.<sup>28</sup> However it is difficult to obtain the diffraction peak with large angle due to preferential orientation of ZnO. Even though the diffraction peak with large angle is observed, its intensity is weak, especially when inclination angle is not zero. Therefore, the strongest diffraction peak, (002), is used to measure biaxial stress in the present work.

#### B. Biaxial tensile stress of ZnO thin films grown on quartz substrate

Figure 4(a) shows XRD plot of as-grown ZnO thin film

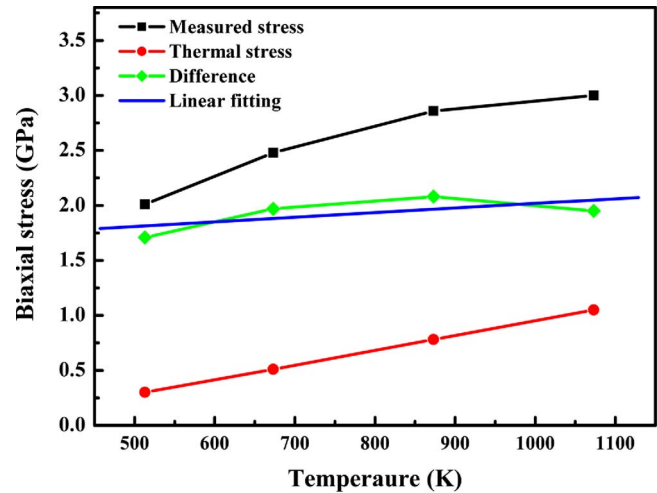


FIG. 5. (Color online) The total and thermal stress as a function of annealing temperature.

at the inclination angles  $\psi=0, 10^\circ, 20^\circ, 30^\circ$ , and  $40^\circ$ . The intensity of (002) diffraction peak rapidly becomes weak with the increase in the inclination angle, indicating that the samples have high (002) preferential orientation. Moreover the (002) diffraction peak shifts to low angle with increasing inclination angle, indicating that the ZnO film is subjected to biaxial tensile stress. The linear relationship between the (002) peak position and  $\sin^2 \psi$  is shown in Fig. 4(b). The stress can be calculated by Eq. (11). Young's module  $E$  and Poisson ratio  $\nu$  adopt the present calculated values 151 GPa and 0.309, which are much close to the experimental values. The measured biaxial stress of all samples as a function of growth or annealing temperature is shown in Fig. 5. It is found that the biaxial tensile stress gradually increases from 2.01 to 3.00 GPa with the increase in annealing temperature from 240 to 800 °C. Meanwhile, the (002) diffraction peaks of annealed ZnO films show obvious shift to large angle with respect to the as-grown sample, as shown in Fig. 6, indicating that the biaxial tensile stress increases after postannealing. This is agreed with the result from the side-inclination XRD method. In some literatures, some researchers measured the biaxial stress of ZnO film by the shift of Bragg's angle with respect to bulk ZnO. The formula can be expressed by the following:<sup>29</sup>

$$\sigma_{xx} = -\frac{2c_{13}^2 - c_{33}(c_{11} - c_{12})}{2c_{13}} \frac{\Delta(2\theta)}{2 \tan \theta_0}. \quad (12)$$

However this method has a disadvantage that the diffraction peak must be precise enough, for example, the diffraction peak is calibrated by the diffraction peak of substrate. In the present work, the ZnO thin film was prepared on quartz substrate. The quartz substrate is an amorphous material that there is no any diffraction peak in XRD pattern. So, the diffraction peak of ZnO film cannot be calibrated. However with the side-inclination XRD method, biaxial stress measurement is not dependent on absolute position of the diffraction peak but relative shift of the peak position at various inclination angles, making the biaxial stress measurement precise and reliable.

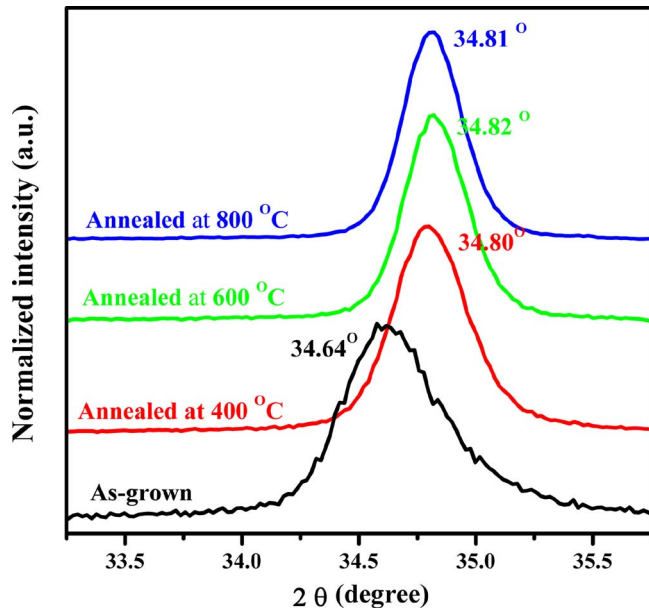


FIG. 6. (Color online) XRD plots of the as-grown and annealed ZnO thin films.

Although the measured value of the biaxial stress at the same annealing temperature has a slight difference between the present and previous work, the change trend of biaxial stress with the increase in annealing temperature is agreed with our previous work.<sup>28</sup> The difference between the present and previous work is due to the choice of different diffraction peaks used to measure biaxial stress. Generally, large tensile stress results in the crack in the surface of film. Figure 7 shows a scanning electron microscopy (SEM) photograph of the sample annealed at 600 °C. The crack on the ZnO surface can be clearly seen due to the biaxial tensile stress. This further confirms that existence of biaxial stress in ZnO thin films, supporting the measurement result of biaxial stress. The biaxial tensile stress originates from the large thermal expansion coefficient difference between ZnO film and quartz substrate. During decreasing temperature, for instance, from growth or annealing temperature to room temperature, shrinkage speed of the quartz substrate is much slower than one of ZnO film owing to thermal expansion

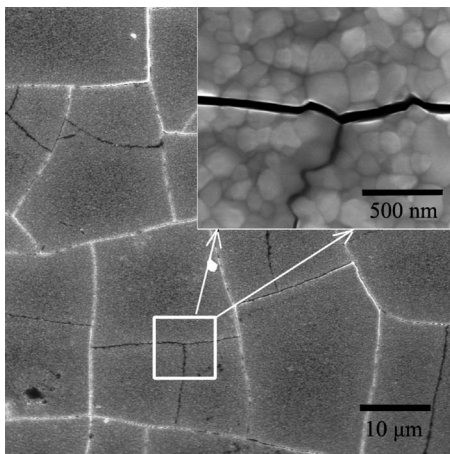


FIG. 7. The SEM photograph of the ZnO thin films annealed at 600 °C.

coefficient of quartz much smaller than one of ZnO film. The shrinkage of ZnO film will be restrained by quartz substrate and then the lattice constant of ZnO film is larger than one of bulk ZnO when decreasing to room temperature. Thus, the biaxial tensile stress occurs in ZnO films grown on quartz substrate.

### C. Thermal stress of ZnO thin films grown on quartz substrate

To well understand the origin of the increase of biaxial tensile stress with increasing annealing temperature, the thermal mismatch stress is calculated for all samples. The thermal mismatch stress can be calculated by the following formula:

$$\sigma_{th} = \int_{T_{growth/anneal}}^{R.T.} (\alpha^f - \alpha^b) \frac{E}{1 - \nu} dT, \quad (13)$$

where  $\alpha^f$  are thermal expansion coefficients of the film deposited on substrate and  $\alpha^b$  are thermal expansion coefficients of the corresponding bulk. If the stress is not relaxed,  $\alpha^f$  can be replaced by the thermal expansion coefficients of the substrate  $\alpha^s$ . Here, the thermal expansion coefficients are considered as a constant within the range of temperature from 240 to 800 °C. The calculated thermal mismatch stress is shown in Fig. 5. The thermal mismatch stress linearly increases with the increase in annealing temperature. Moreover the difference between measured stress and thermal mismatch stress is also shown in Fig. 5. The change range of the difference for all samples is from 1.71 to 2.08 GPa and the slope of linear fitting to the differences is almost zero. This indicates the difference is a constant (average value is 1.93 GPa) and not related to annealing temperature. Therefore, the increase in biaxial tensile stress with annealing temperature is due to the increase in thermal stress with annealing temperature.

It is well known that the residual stress is not only related to the macroscopical stress but also microscopical stress. The macroscopical stress, such as lattice mismatch and thermal mismatch stress, is related to the whole film. Differing from macroscopical stress, the microscopical stress originates from local nonuniformity in the film, such as local defects or impurities, which results in different interplanar distances for the same crystal planar index at different regions. Thus, the shape of diffraction peak will widen. However, the widening of shape is also related to grain size. Excluding the effect of grain size on widening of shape, the microscopic stress can be estimated by full width at half maximum (FWHM) of diffraction peak. The microscopic stress of thin film can be calculated by the following:

$$\sigma = \frac{E(\beta - K\lambda/L \cos \theta)}{4 \tan \theta}. \quad (14)$$

The FWHM ( $\beta$ ) of the (002) diffraction peak of ZnO films as a function of annealing temperature is shown in Fig. 8. It is found that the FWHM increases with the increase in annealing temperature. Meanwhile, the average grain size enlarges from 50 to 100 nm when annealing temperature increases from 240 to 800 °C. As a result, the microscopical

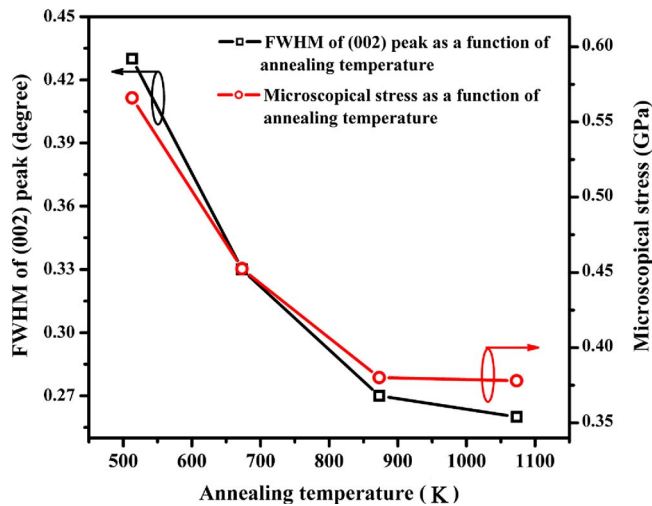


FIG. 8. (Color online) FWHM of (002) diffraction peak and microscopical stress of ZnO films as a function of annealing temperature.

stress is small and decreases from 0.56 to 0.38 GPa with increasing annealing temperature, as shown in Fig. 8. Moreover the change in microscopical stress (0.18 GPa) is smaller than that of macroscopical stress ( $\sim 1$  GPa). Therefore, the microscopical stress can be neglected with respect to macroscopical stress.

On the other hand, it is known that the biaxial stress of film is strongly dependent on its thickness under some condition. For example, the large stress remains in the thin film when the thickness of thin film is thinner than the critical thickness because the epilayer has the same lattice constant with the substrate. The deformation energy increases with the increase in the film thickness. Because the deformation energy cannot be unlimitedly accumulated, the stress will be rapidly relaxed when the thickness of thin film is over the critical thickness. In order to make it clear if the annealed ZnO films become thinner and if the thinner films result in the increase in the biaxial stress, the thickness of as-grown, and all annealed samples were measured by SEM. Figure 9 shows the thickness of all samples. The as-grown and annealed ZnO films have a same thickness of 1200 nm. This is due to the following reasons: (i) the annealing time is not long enough to the thinner film and (ii) the  $O_2$  atmosphere can suppress the host material (Zn and O) escaping from the thin films. Therefore, the effect of thickness on biaxial stress is excluded. Furthermore, in the present work, the ZnO film was deposited on quartz substrate which is an amorphous material. An amorphous material has not a certain lattice. Hence, the concept on critical thickness is not suitable for the present work.

#### D. The relationship between band gap and biaxial tensile stress of ZnO thin films

To obtain the relationship between the biaxial stress and band gap, the optical band gaps of all samples are determined by performing optical absorption spectrum. Figures 10(a) and 10(b) show the absorption spectra of all samples and optical band gap as a function of biaxial tensile stress, respectively. The measured band gap increases from 3.225 to

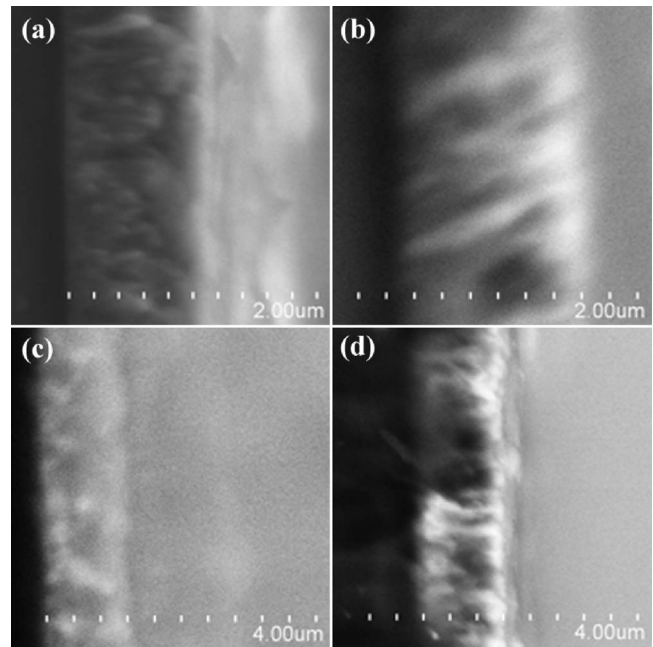


FIG. 9. The thickness of the as-grown and annealed ZnO thin films.

3.255 eV with the increase in biaxial tensile stress from 2.01 to 3.00 GPa. We obtained the linear relationship between the band gap and biaxial as follows:

$$E_g = 3.171 + 0.027\sigma_{xx}, \quad (15)$$

where 3.171 eV is optical band gap of stress-free ZnO thin film. The value is obviously smaller than one of bulk ZnO. The inset in Fig. 7 shows the grain in ZnO films, confirming that the samples are polycrystalline. The barriers at grain boundary make effect band gap decrease.<sup>30</sup> As a result, the band gap of stress-free is smaller than bulk ZnO. The stress coefficient, 27 meV/GPa, is smaller than the previous work, which is due to different stress values obtained using different diffraction peaks.<sup>28</sup>

In the case of the effect of biaxial stress on band gap, ZnO film differs from GaN film which has a same crystalline structure with ZnO. Zhao *et al.*<sup>31</sup> investigated the relation-

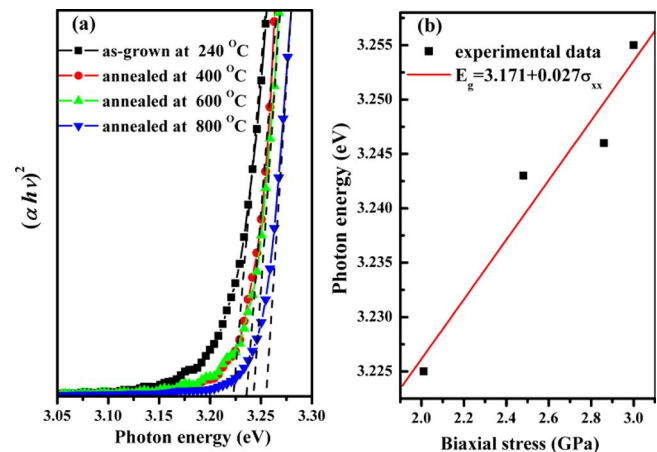


FIG. 10. (Color online) (a) Optical absorption spectrum of the as-grown ZnO thin film and annealed at 400, 600, and 800 °C. (b) The linear relationship between optical band gap and biaxial tensile stress of ZnO thin films.



TABLE II. Structural parameters of wurtzite ZnO and GaN.

|                    | <i>a</i><br>(nm) | <i>c</i><br>(nm) | <i>c/a</i> | <i>u</i> |
|--------------------|------------------|------------------|------------|----------|
| ZnO                |                  |                  |            |          |
| Present            | 0.3252           | 0.5251           | 1.615      | 0.379    |
| Calc. <sup>a</sup> | 0.3270           | 0.5240           | 1.602      | 0.381    |
| Expt. <sup>b</sup> | 0.3250           | 0.5204           | 1.601      | 0.382    |
| GaN                |                  |                  |            |          |
| Present            | 0.3201           | 0.5215           | 1.629      | 0.377    |
| Calc. <sup>c</sup> | 0.3220           | 0.5260           | 1.634      | 0.371    |
| Expt. <sup>d</sup> | 0.3190           | 0.5189           | 1.627      | 0.377    |

<sup>a</sup>Reference 37.<sup>b</sup>Reference 38.<sup>c</sup>Reference 38.<sup>d</sup>Reference 40.

ship between band gap and biaxial stress of GaN in experiments. It is found that the band gap of wurtzite GaN decreases with the increase in biaxial tensile stress or with the decrease in biaxial compressive stress. The difference between ZnO and GaN will be discussed in Sec. IV.

#### IV. BIAxIAL STRESS-DEPENDENT CRYSTALLINE AND ELECTRONIC STRUCTURE OF WURTZITE ZINC OXIDE AND GALLIUM NITRIDE: A COMPARATIVE STUDY BASED ON *AB INITIO* CALCULATION

In order to well understand the difference between ZnO and GaN, *ab initio* calculation is performed to simulate the relationship between band gap and biaxial stress.

##### A. Computational detail

The DFT<sup>32,33</sup> in the generalized gradient approximation (PW91 GGA) (Ref. 34) and ultrasoft pseudopotentials<sup>35,36</sup> with a plane-wave basis set are used to perform the *ab initio* calculation. The crystalline structure of ZnO and GaN are optimized by using the CASTEP code<sup>37</sup> in which the total

energy is minimized from all atomic configurations. The O  $2s^2 2p^4$ , Zn  $3d^{10} 4s^2$ , N  $2s^2 2p^3$ , and Ga  $3d^{10} 4s^2 4p^1$ , with core electrons, were treated as valence electrons in the calculation. For obtaining high levels of precision, the plane-wave basis set cut-off energy of 700 eV was used. Moreover for *k*-point sampling, a  $9 \times 9 \times 6$  Monkhorst-Pack mesh in the Brillouin zone was employed.

The structure of wurtzite crystal (space group  $P6_3mc$ ) is hexagonal with four atoms in primitive unit cell and with two lattice constants *a* and *c*, which is shown in Fig. 1. The experimental lattice constants,  $a=0.3249$  and  $c=0.5205$  nm as well as  $a=0.3190$  and  $c=0.5189$  nm, were used to construct two initial primitive cells for ZnO and GaN, respectively. The optimized structural parameters are listed in Table II. The optimized lattice constants are close to the calculated ones by Yu *et al.*<sup>38</sup> and Vogel *et al.*<sup>39</sup> Comparing with the experimental results,<sup>40,41</sup> the error is smaller than 0.1%.

##### B. Effect of biaxial stress on crystalline structure of ZnO and GaN

It is very easy to form wurtzite structure with *c*-axis preferentially orientation (*c*-axis perpendicular to substrate surface), for ZnO and GaN thin films grown on common insulation or semiconductor substrate, such as *c*-sapphire,<sup>42,43</sup> quartz,<sup>44,45</sup> Si (111),<sup>46,47</sup> and GaAs (111),<sup>48</sup> by various physical and chemical methods, for example, molecular beam epitaxy, pulse laser deposition, metal-organic vapor phase deposition, and magnetic sputtering method. Therefore, to simulate the biaxial stress of wurtzite ZnO and GaN thin films grown on these substrates, the stress tensor elements are set to  $\sigma_{11}=\sigma_{22}=\sigma$  and  $\sigma_{33}=\sigma_{ij}=0$  ( $i \neq j$ ). Because the thin films in *c*-axis direction are not restricted, the condition  $\sigma_{33}=0$  is adopted.

The lattice constants *a* and *c* of wurtzite ZnO and GaN under different biaxial stresses are shown in Fig. 11(a). The lattice constant *a* increases with decreasing biaxial compressive stress and with increasing biaxial tensile stress for ZnO

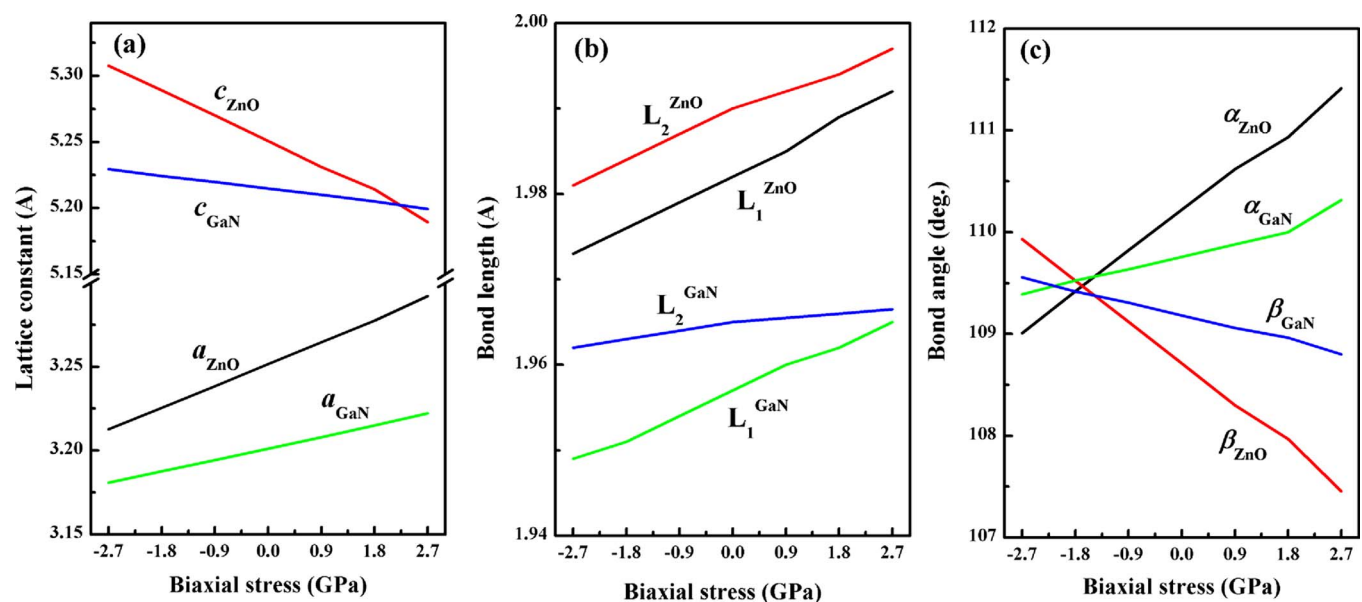


FIG. 11. (Color online) (a) Lattice constants, (b) bond lengths, and (c) bond angles as a function of biaxial stress for ZnO and GaN.



and GaN. However the lattice constant  $c$  decreases due to the Poisson effect. The slopes of lines  $a_{\text{ZnO}}$  and  $c_{\text{ZnO}}$  are larger than those of lines  $a_{\text{GaN}}$  and  $c_{\text{GaN}}$ , respectively, indicating that the change in lattice constants of ZnO with biaxial stress is larger than one of GaN. This is because the elastic constants of ZnO are larger than that of GaN. In order to be sure if the decrease in  $c$ -axial lattice constants of ZnO and GaN is induced by the decrease in bond length along  $c$ -axis, the change in bond length and bond angle under biaxial stress is also studied. As shown in Fig. 1, there are four bonds in tetrahedron, three of them have the same bond length and the other is along  $c$ -axis, their bond lengths are labeled  $L_1$  and  $L_2$ , respectively. Three of four bond angles are also the same, labeled as  $\alpha$ . The other is labeled as  $\beta$ . The relationship between lattice constant and bond length as well as bond angle can be expressed by the following equations:

$$a = 2L_1 \sin \frac{\alpha}{2}, \quad (16a)$$

$$c = 2L_2 - 2L_1 \cos \beta. \quad (16b)$$

The bond lengths of wurtzite ZnO and GaN as a function of the biaxial stress are shown in Fig. 11(b). For ZnO and GaN, besides the bond length  $L_1$  increases with the decrease in biaxial compressive stress and with the increase in biaxial tensile stress, the bond length  $L_2$  also increases. According to Eq. (16b), the increase in  $L_1$  and  $L_2$  indicates that the bond angle  $\beta$  must be decreased. Figure 11(c) shows bond angle  $\alpha$  and  $\beta$  as a function of biaxial stress. The bond angle  $\beta$  decreases with the increase in biaxial tensile stress. Thus, the decrease in lattice constant  $c$  originates from the decrease of angle  $\beta$  but not the decrease in bond length  $L_2$ . It is well known that the bond length is directly related to the intensity of interaction. Under biaxial tensile stress, both bond lengths  $L_1$  and  $L_2$  increase, indicating that the intensity of interaction between cation and anion is decreased.

### C. Effect of biaxial stress on electronic structure of ZnO and GaN

The linear relationship of between band gap and biaxial stress of wurtzite ZnO and GaN is shown in Fig. 12. The calculated band gaps of stress-free ZnO and GaN are 0.986 and 1.982 eV, in agreement with the others' calculated results by GGA method.<sup>49,50</sup> The band gap of ZnO increases with the decrease in biaxial compressive stress and with the increase in biaxial tensile stress. The linear relationship between band gap and biaxial stress is expressed as the following:

$$E_g = 0.984 + 0.003\sigma_{11}. \quad (17)$$

In the case of the change trend of band gap with biaxial stress, this result is agreed with the experiment in Sec. V, supporting our experimental result. Recently, Alahmed and Fu<sup>51</sup> also studied the effect of biaxial strain with band gap of ZnO using local density approximation method. Their results agreed with ours. However, the biaxial stress-dependent band gap of GaN is opposite to that of ZnO. The linear relation-

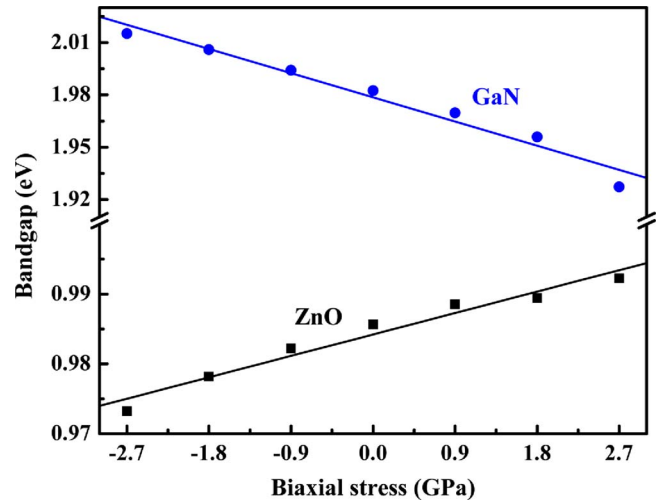


FIG. 12. (Color online) Calculated band gap as a function of biaxial stress of ZnO and GaN.

ship between band gap and biaxial stress is expressed as the following:

$$E_g = 1.979 - 0.015\sigma_{11}. \quad (18)$$

The biaxial stress coefficient with a minus indicates that the band gap of GaN decreases with the increase in biaxial tensile stress.

To explain the difference between ZnO and GaN, the alignment of the valence-band maximum (VBM) and conduction-band minimum (CBM) induced by biaxial stress must be obtained. For the alignment of the VBM, it is necessary to obtain the average electrostatic potential in the supercell approach or to choose the proper core level as reference.<sup>52,53</sup> Here, we choose the core level of O  $2s$  state with low energy as reference to align the VBM. The alignment of CBM and VBM of ZnO and GaN is shown in Fig. 13. The CBM and VBM of ZnO and GaN offset to low energy under biaxial tensile stress. For ZnO, the offset of VBM is larger than that of CBM, indicating the increase in band gap. The offset of VBM is about 15 times than the increment of band gap. However for GaN, the offset of VBM is smaller than that of CBM, indicating the decrease in band gap. The offset of VBM is only 1.2 times than the change in

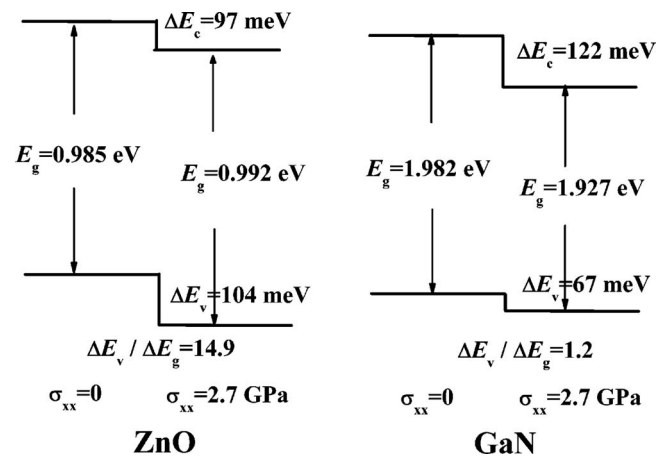


FIG. 13. Calculated alignment of CBM and VBM of (a) ZnO and (b) GaN.

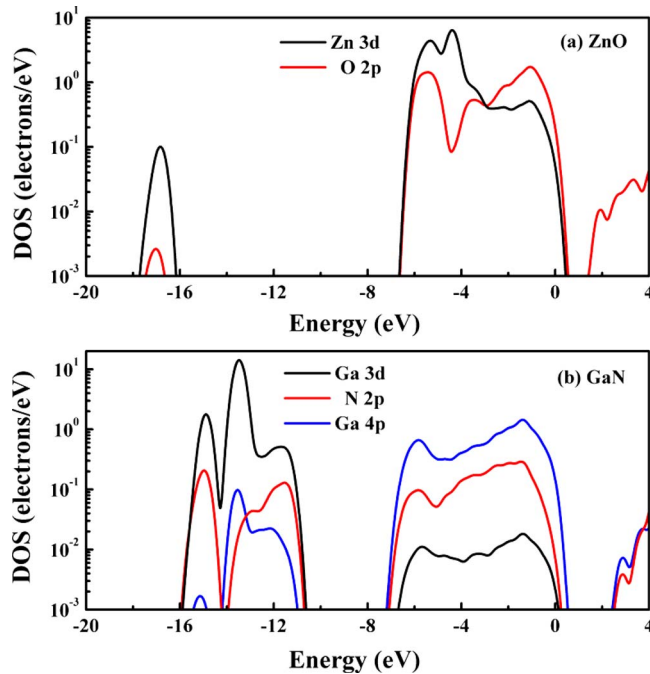


FIG. 14. (Color online) Calculated partial density of state of (a) ZnO and (b) GaN.

band gap. Therefore, under the biaxial tensile stress, the difference in change in band gap between ZnO and GaN can be attributed to the large VBM offset of ZnO.

According to the tight-binding approach model, the band offset is attributed to two effects: (i) the kinetic energy effect and (ii) the bond and antibond state effects.<sup>54</sup> The kinetic energy decreases as bond length increases. Because the long bond length means weak interaction, the energy increases with the increase in bond length for bond states and the energy decreases with the increase in bond length for antibond states. As discussed above, under biaxial tensile, the decrease in both bond lengths  $L_1$  and  $L_2$  indicates the decrease in intensity of interaction. Generally, the CBM is an antibond state due to the interaction between the cation- $s$  and anion- $s$  valence orbitals. Thus, under biaxial tensile stress, the CBM of ZnO and GaN offsets to low energy because of the kinetic energy effect and the antibond state effect. However VBM is generally a bond state due to the interaction between the anion- $p$  and cation- $p$  valence orbitals. Thus, offset of VBM is generally small because of the competition between kinetic energy effect and bond state effect, namely, the two effects partially cancel each other. This can explain the VBM offset of GaN under biaxial tensile stress. However, the VBM offset of ZnO is very large ( $\Delta E_v/\Delta E_g \approx 15$ ). The reason is speculated that the VBM of ZnO is an antibond state because of the interaction between anion- $p$  and cation- $d$  valence orbitals. In order to confirm our speculation, the densities of state for ZnO and GaN are calculated. Figure 14 shows the partial density of state of ZnO and GaN. The energy of 3d electrons of Zn is closed to that of 2p electrons of O in the valence band, indicating that the anion- $p$  and cation- $d$  couplings in ZnO are strong. However the energy of 3d electrons of Ga is much lower than that of 2p electrons of N, indicating that the  $p$ - $d$  coupling in GaN is very weak.

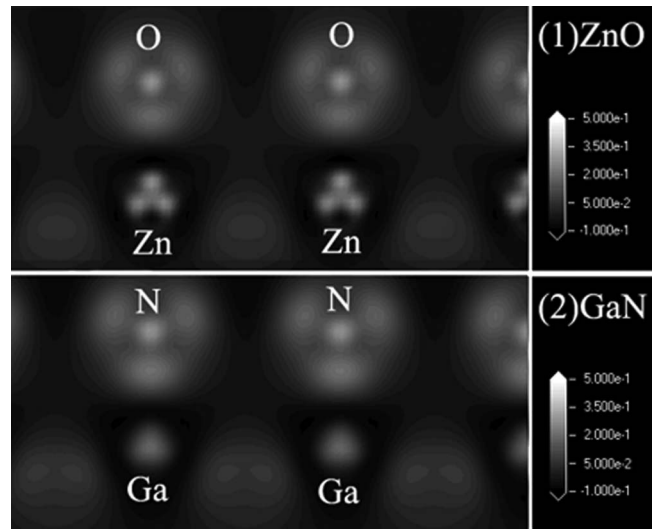


FIG. 15. Calculated charge density plot of ZnO and GaN.

There is strong cation- $p$  and anion- $p$  coupling in valence band of GaN. Figure 15 shows the charge density plot of ZnO and GaN. The shape of the 3d electron cloud of Ga is almost a sphere, indicating that the 3d electrons are very local and their energy is very low, in agreement with the calculated state of density. However the 3d electron cloud of Zn is obviously extended to four directions, pointing to near four O atoms, respectively. Hence, the interaction of Zn 3d electrons and O 2p electrons is strong. The more local 3d electrons of Ga in GaN than that of Zn in ZnO is because the proton number of Ga atomic nucleus is more one than that of Zn atomic nucleus. The atomic nucleus of Ga has stronger attraction to 3d electrons than that of Zn.

As a result, under biaxial tensile stress, the band gap of ZnO increases but that of GaN decreases. The VBM and CBM of both ZnO and GaN offset to low energy under biaxial tensile stress. The increase in band gap of ZnO originates from the larger VBM offset than CBM offset. However, the decrease in band gap of GaN originates from the smaller VBM offset than CBM offset. The difference in biaxial stress-dependent band gap of ZnO and GaN is attributed to the large VBM offset of ZnO because of strong  $p$ - $d$  coupling in valence band.

## V. CONCLUSION

In summary, we obtain the relationship between band gap and biaxial stress of ZnO thin films by side-inclination XRD technique and optical absorbance spectrum. The band gap of ZnO thin films increases with the increase in biaxial tensile stress, differing from wurtzite GaN. The results from *ab initio* calculation indicate that the band gap of ZnO increases under biaxial tensile stress but GaN is opposite, supporting our experimental results. The band offset calculation shows that the CBM and the VBM of ZnO and GaN offset to low energy under biaxial tensile stress. The VBM offset of ZnO is larger than the CBM, indicating the band gap increases. Moreover the VBM offset of GaN is smaller than the CBM, indicating that the band gap decreases. The difference between ZnO and GaN is attributed to large VBM offset of

ZnO to low energy. The strong  $p$ - $d$  coupling in valence band of ZnO is responsible for the large VBM offset.

## ACKNOWLEDGMENTS

This work was supported by the Key Project of National Natural Science Foundation of China under Grant Nos. 60336020 and 50532050, the “973” Program under Grant No. 2006CB604906, the Innovation Project of Chinese Academy of Sciences, and the National Natural Science Foundation of China under Grant Nos. 60429403, 60506014, 50402016, 10674133, and 60776011.

- <sup>1</sup>D. C. Look, *Mater. Sci. Eng., B* **80**, 383 (2001).
- <sup>2</sup>A. Tsukazaki, T. Onuma, M. Ohtani, T. Makino, M. Sumiya, K. Ohtani, S. F. Chichibu, S. Fuke, Y. Segawa, H. Ohno, H. Koinuma, and M. Kawasaki, *Nature Mater.* **4**, 42 (2005).
- <sup>3</sup>S. J. Jiao, Z. Z. Zhang, Y. M. Lu, D. Z. Shen, B. Yao, J. Y. Zhang, B. H. Li, D. X. Zhao, X. W. Fan, and Z. K. Tang, *Appl. Phys. Lett.* **88**, 031911 (2006).
- <sup>4</sup>Z. P. Wei, Y. M. Lu, D. Z. Shen, Z. Z. Zhang, B. Yao, B. H. Li, J. Y. Zhang, D. X. Zhao, X. W. Fan, and Z. K. Tang, *Appl. Phys. Lett.* **90**, 042113 (2007).
- <sup>5</sup>Y. Ryu, T.-S. Lee, J. A. Lubguban, H. W. White, B.-J. Kim, Y.-S. Park, and C.-J. Youn, *Appl. Phys. Lett.* **88**, 241108 (2006).
- <sup>6</sup>Y. R. Ryu, J. A. Lubguban, T. S. Lee, H. W. White, T. S. Jeong, C. J. Youn, and B. J. Kim, *Appl. Phys. Lett.* **90**, 131115 (2007).
- <sup>7</sup>L. J. Mandalapu, Z. Yang, S. Chu, and J. L. Liu, *Appl. Phys. Lett.* **92**, 122101 (2008).
- <sup>8</sup>Y.-L. Wang, H. S. Kim, D. P. Norton, S. J. Pearton, and F. Ren, *Appl. Phys. Lett.* **92**, 112101 (2008).
- <sup>9</sup>Z. Z. Ye, J. G. Lu, Y. Z. Zhang, Y. J. Zeng, L. L. Chen, F. Zhuge, G. D. Yuan, H. P. He, L. P. Zhu, J. Y. Huang, and B. H. Zhao, *Appl. Phys. Lett.* **91**, 113503 (2007).
- <sup>10</sup>S. Nakamura, S. Pearton, and G. Fasol, *The Blue Laser Diode* (Springer, Berlin, 2000).
- <sup>11</sup>M. Lopuszynski and J. A. Majewski, *Phys. Rev. B* **76**, 045202 (2007).
- <sup>12</sup>J. Sun, H.-T. Wang, J. He, and Y. Tian, *Phys. Rev. B* **71**, 125132 (2005).
- <sup>13</sup>F. Decrempe, J. Pellicer-Porres, A. M. Saitta, J.-C. Chervin, and A. Polian, *Phys. Rev. B* **65**, 092101 (2002).
- <sup>14</sup>W. Shan, T. J. Schmidt, R. J. Hauenstein, J. J. Song, and B. Goldenberg, *Appl. Phys. Lett.* **66**, 3492 (1995).
- <sup>15</sup>W. Shan, W. Walukiewicz, J. W. Ager III, K. M. Yu, Y. Zhang, S. S. Mao, R. Kling, C. Kirchner, and A. Waag, *Appl. Phys. Lett.* **86**, 153117 (2005).
- <sup>16</sup>M. P. Halsall, P. Harmer, P. J. Parbrook, and S. J. Henley, *Phys. Rev. B* **69**, 235207 (2004).
- <sup>17</sup>Z. C. Tu and X. Hu, *Phys. Rev. B* **74**, 035434 (2006).
- <sup>18</sup>X. Wu, D. Vanderbilt, and D. R. Hamann, *Phys. Rev. B* **72**, 035105 (2005).
- <sup>19</sup>M. Catti, Y. Noel, and R. Dovesi, *J. Phys. Chem. Solids* **64**, 2183 (2003).
- <sup>20</sup>T. B. Bateman, *J. Appl. Phys.* **33**, 3309 (1962).
- <sup>21</sup>I. B. Kobiakov, *Solid State Commun.* **35**, 305 (1980).
- <sup>22</sup>T. Azuhata, M. Takesada, T. Yagi, A. Shikanai, S. F. Chichibu, K. Torii, A. Nakamura, T. Sota, G. Cantwell, D. B. Eason, and C. W. Litton, *J. Appl. Phys.* **94**, 968 (2003).
- <sup>23</sup>A. F. Wright, *J. Appl. Phys.* **82**, 2833 (1997).
- <sup>24</sup>K. Shimada, T. Sota, and K. Suzuki, *J. Appl. Phys.* **84**, 4951 (1998).
- <sup>25</sup>K. Kim, W. R. L. Lambrecht, and B. Segall, *Phys. Rev. B* **50**, 1502 (1994).
- <sup>26</sup>C. Deger, E. Born, H. Angerer, O. Ambacher, M. Stutzmann, J. Hornsteiner, E. Riha, and G. Fischerauer, *Appl. Phys. Lett.* **72**, 2400 (1998).
- <sup>27</sup>M. Yamaguchi, T. Yagi, T. Sota, T. Deguchi, K. Shimada, and S. Nakamura, *J. Appl. Phys.* **85**, 8502 (1999).
- <sup>28</sup>Y. F. Li, B. Yao, Y. M. Lu, C. X. Cong, Z. Z. Zhang, C. J. Zheng, B. H. Li, Z. P. Wei, D. Z. Shen, X. W. Fan, L. Xiao, S. C. Xu, and Y. Liu, *Appl. Phys. Lett.* **91**, 021915 (2007).
- <sup>29</sup>V. Gupta and A. Mansingh, *J. Appl. Phys.* **80**, 1063 (1996).
- <sup>30</sup>V. Srikant and D. R. Clarke, *J. Appl. Phys.* **81**, 6357 (1997).
- <sup>31</sup>D. G. Zhao, S. J. Xu, M. H. Xie, S. Y. Tong, and H. Yang, *Appl. Phys. Lett.* **83**, 677 (2003).
- <sup>32</sup>P. Hohenberg and W. Kohn, *Phys. Rev.* **136**, 864 (1964).
- <sup>33</sup>W. Kohn and L. J. Sham, *Phys. Rev.* **140**, A1133 (1965).
- <sup>34</sup>J. P. Perdew, J. A. Chevary, S. H. Vosko, K. A. Jackson, M. R. Pederson, D. J. Singh, and C. Fiolhais, *Phys. Rev. B* **46**, 6671 (1992).
- <sup>35</sup>D. Vanderbilt, *Phys. Rev. B* **41**, 7892 (1990).
- <sup>36</sup>K. Laasonen, R. Car, C. Lee, and D. Vanderbilt, *Phys. Rev. B* **43**, 6796 (1991).
- <sup>37</sup>M. D. Segall, P. J. D. Lindan, M. J. Probert, C. J. Pickard, P. J. Hasnip, S. J. Clark, and M. C. Payne, *J. Phys.: Condens. Matter* **14**, 2717 (2002).
- <sup>38</sup>Z. G. Yu, H. Gong, and P. Wu, *J. Cryst. Growth* **287**, 199 (2006).
- <sup>39</sup>D. Vogel, P. Kruger, and J. Pollmann, *Phys. Rev. B* **55**, 12836 (1997).
- <sup>40</sup>H. Karzel, W. Potzel, M. Köfferlein, W. Schiessl, M. Steiner, U. Hiller, G. M. Kalvius, D. W. Mitchell, T. P. Das, P. Blaha, K. Schwarz, and M. P. Pasternak, *Phys. Rev. B* **53**, 11425 (1996).
- <sup>41</sup>H. Schulz and K. H. Thiemann, *Solid State Commun.* **23**, 815 (1977).
- <sup>42</sup>F. K. Shan, G. X. Liu, W. J. Lee, and B. C. Shin, *J. Appl. Phys.* **101**, 053106 (2007).
- <sup>43</sup>A. Dissanayake, J. Y. Lin, H. X. Jiang, Z. J. Yu, and J. H. Edgar, *Appl. Phys. Lett.* **65**, 2317 (1994).
- <sup>44</sup>B. Yao, D. Z. Shen, Z. Z. Zhang, X. H. Wang, Z. P. Wei, B. H. Li, Y. M. Lu, X. W. Fan, L. X. Guan, G. Z. Xing, C. X. Cong, and Y. P. Xie, *J. Appl. Phys.* **99**, 123510 (2006).
- <sup>45</sup>B. S. Yadav, S. S. Major, and R. S. Srinivasa, *J. Appl. Phys.* **102**, 073516 (2007).
- <sup>46</sup>Z. G. Zhang, F. Zhou, X. Q. Wei, M. Liu, G. Sun, C. S. Chen, C. S. Xue, H. Z. Zhuang, and B. Y. Man, *Physica E (Amsterdam)* **39**, 253 (2007).
- <sup>47</sup>N. Chaaben, T. Boufaden, A. Fouzri, M. S. Bergaoui, and B. El Jani, *Appl. Surf. Sci.* **253**, 241 (2006).
- <sup>48</sup>H. F. Liu, S. J. Chua, G. X. Hu, H. Gong, and N. Xiang, *J. Appl. Phys.* **102**, 083529 (2007).
- <sup>49</sup>A. Schleife, F. Fuchs, J. Furthmüller, and F. Bechstedt, *Phys. Rev. B* **73**, 245212 (2006).
- <sup>50</sup>G. Y. Gao, K. L. Yao, Z. L. Liu, Y. L. Li, Y. C. Li, and Q. M. Liu, *Solid State Commun.* **138**, 494 (2006).
- <sup>51</sup>Z. Alahmed and H. Fu, *Phys. Rev. B* **77**, 045213 (2008).
- <sup>52</sup>C. G. Van de Walle and R. M. Martin, *Phys. Rev. B* **35**, 8154 (1987).
- <sup>53</sup>Y.-H. Li, X. G. Gong, and S.-H. Wei, *Appl. Phys. Lett.* **88**, 042104 (2006).
- <sup>54</sup>A. Janotti and C. G. Van de Walle, *Phys. Rev. B* **75**, 121201(R) (2007).